JCTC Journal of Chemical Theory and Computation

Article

pubs.acs.org/JCTC

Spin-Free CC2 Implementation of Induced Transitions between Singlet Ground and Triplet Excited States

Benjamin Helmich-Paris,*[,†,‡] Christof Hättig,*[,†] and Christoph van Wüllen*[,§]

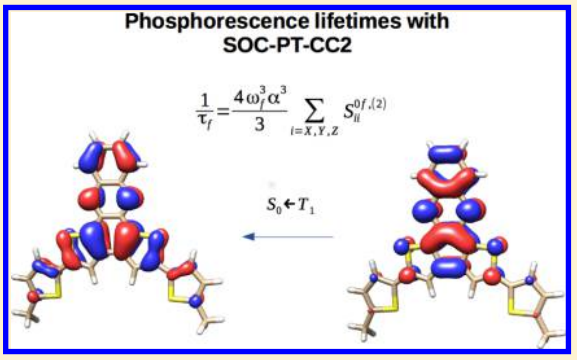
[†]Lehrstuhl für Theoretische Chemie, Ruhr-Universität Bochum, 44801 Bochum, Germany

[‡]Section of Theoretical Chemistry, VU University Amsterdam, De Boelelaan 1083, 1081 HV Amsterdam, The Netherlands

[§]TU Kaiserslautern, FB Chemie and Forschungszentrum OPTIMAS, Erwin-Schrödinger-Str. 52, D-67663 Kaiserslautern, Germany

Supporting Information

ABSTRACT: In most organic molecules, phosphorescence has its origin in transitions from triplet exited states to the singlet ground state, which are spin-forbidden in nonrelativistic quantum mechanics. A sufficiently accurate description of phosphorescence lifetimes for molecules that contain only light elements can be achieved by treating the spin−orbit coupling (SOC) with perturbation theory (PT). We present an efficient implementation of this approach for the approximate coupled cluster singles and doubles model CC2 in combination with the resolution-of-the-identity approximation for the electron repulsion integrals. The induced oscillator strengths and phosphorescence lifetimes from SOC-PT are computed within the response theory framework. In contrast to previous work, we employ an explicitly spin-coupled basis for singlet and triplet operators. Thereby, a spin−orbital treatment can be entirely avoided for closed-shell molecules. For compounds containing only light elements, the phosphorescence lifetimes obtained with SOC-PT-CC2 are in good agreement with those of exact two-component (X2C) CC2, whereas the calculations are roughly 12 times faster than with X2C. Phosphorescence lifetimes computed for two thioketones with the SOC-PT-CC2 approach agree very well with reference results from experiment and are similar to those obtained with multireference spin−orbit configuration interaction and with X2C-CC2. An application to phosphorescent emitters for metal-free organic light-emitting diodes (OLEDs) with almost 60 atoms and more than 1800 basis functions demonstrates how the approach extends the applicability of coupled cluster methods for studying phosphorescence. The results indicate that other decay channels like vibrational relaxation may become important in such systems if lifetimes are large.



I. INTRODUCTION

Phosphorescence is the emission of light accompanied by a change in the electronic spin quantum number. In most cases, the excited electrons undergo a transition from the lowest excited triplet states to the singlet ground state. In spectroscopy, those triplet states were populated before by intersystem crossing or internal conversion from higher excited states. Among other competing transition processes, for example, fluorescence, internal conversion from higher states, and vibrational relaxation, one must account for phosphorescence as well to understand the fate of excited electronic states. For compounds containing only light elements, phosphorescence is usually several orders of magnitude slower than other decay processes. If those competing, both radiative and nonradiative, processes are suppressed, a long-lasting *glow-in-the-dark* effect is observed. In recent years, an interest in a thorough understanding of singlet−triplet transitions has been enforced by the development of organic light-emitting diodes (OLEDs). They exploit organic phosphors to implement full-color displays in all kinds of electronic devices.[1]

Transitions between electronic states with different multiplicity are spin-forbidden in nonrelativistic quantum mechanics, but they are spin-allowed in extended theories that account for relativity. Only the inclusion of spin-dependent terms into the nonrelativistic Hamiltonian leads to a coupling of spin and orbital angular momenta, the so-called spin−orbit coupling (SOC), which induces "spin-forbidden" transitions. Currently, the most rigorous way to account for relativistic effects in atoms and molecules is to solve the Dirac equation with four-component (4C) wave functions. Although we can account for relativity with the 4C Dirac equation, this has two major drawbacks. First, besides the positive electronic solutions, one gets a negative energy continuum of positronic states that are in most cases meaningless for chemistry. Besides, it is unclear whether and how negative-energy orbitals have to be included in the correlation treatment. Second, the computational costs for 4C wave function calculations are much larger than for nonrelativistic one-component (1C) calculations. An approximation that addresses both issues by decoupling of the electronic from the positronic states is the exact two-component (X2C) ansatz.[2] Though the overhead of using a

Received: December 17, 2015
Published: February 16, 2016

Downloaded via BOCHUM LIBRARIES on January 16, 2019 at 10:09:41 (UTC).
See https://pubs.acs.org/sharingguidelines for options on how to legitimately share published articles.

© 2016 American Chemical Society

DOI: 10.1021/acs.jctc.5b01197
J. Chem. Theory Comput. 2016, 12, 1892−1904

Dirac−Hamiltonian is reduced by the X2C method, it can still be quite costly in particular for correlated wave function methods. For a thorough discussion on the Dirac equation and its approximations, we refer to the literature.[3]

For molecules with only light elements, SOC effects are small. This allows a separation of scalar-relativistic (SR) and SOC terms of the Dirac−Hamiltonian. By doing this, only the SR part can be included to find a zeroth-order solution in a first step. In a second step, SOC effects can be introduced either variationally by a spin−orbit configuration interaction (SOCI) procedure[4,5] or perturbationally by using, for example, the methodological framework of response theory. In general, SOCI is not strictly size extensive even if semiempirical Hamiltonians are employed.[5,6] A computational attractive approach is to treat SOC as perturbation and compute SOC related phenomena by response theory.[7] Employing response theory together with a SOC perturbation theory (PT) can avoid the size-extensivity issue. Furthermore, it is even more economic than SOCI and avoids truncation errors from slowly converging sum-over-states expressions.[8] From the residues of the linear and quadratic response function, one can calculate SOC matrix elements between different states[9,10] and phosphorescence lifetimes.[11−13] Note that transition moments between (predominantly) singlet and triplet excited states can be obtained directly (without SOC-PT or SOCI) from the residues of the linear response function for 4C or 2C wave functions,[14,15] which is inevitable for the heavier elements.

In many of the SOCI and SOC-PT investigations carried out so far, the SOC operator is used in the Breit−Pauli (BP) form, which includes the spin-same-orbit and spin-other-orbit two-electron integrals. An economic but still accurate approximation is to use an effective one-electron SOC operator that includes the two-electron contributions in a mean-field fashion. The matrix elements of this (effective) one-electron operator are constructed from the one- and two-electron spin−orbit integrals in a similar way the Fock matrix is constructed from the conventional one- and two-electron integrals. This spin−orbit mean-field (SOMF) approach[16−18] can be simplified further to the computationally cheap atomic mean field interaction approximation[17,19,20] (AMFI), which neglects multicenter contributions. Note that in this case, multicenter contributions also have to be eliminated from the one-electron spin−orbit integrals to get a balanced description. However, the computation of SOMF matrix elements can be done efficiently using integral-direct and screening techniques and usually does not take longer than a few self-consistent field (SCF) cycles. Thus, there is no need anymore to employ less robust one-center approximations for the two-electron terms as, for example, in the AMFI approach, especially if correlated wave function methods are used that have a steeper cost-scaling than the SOMF integral evaluation. However, also at the SCF and DFT level, modern integral approximations allow the avoidance of one-center approximations without limiting the applicability range of calculations.[18]

A SOC-PT ansatz that determines singlet−triplet transitions matrix elements within the response theory framework has already been implemented for multiconfigurational SCF[11] (MCSCF), density functional theory[13] (DFT), and the coupled cluster singles and doubles (CCSD) method.[12] Because we are interested in phosphorescence-related phenomena of medium-sized systems, for example, organic phosphors used as dyes for OLEDs, MCSCF, and CCSD are generally not applicable due to their steep scaling of the computational costs with the system size. Excited-state calculations for molecules with more than 100 atoms can nowadays be routinely done with time-dependent DFT,[21] where eventually the computational effort scales linearly with system size.[22] For such large systems, however, charge transfer (CT) excitations are frequently found in the low-energy range of the electronic spectrum and standard semilocal density functionals underestimate excitation energies for these states drastically. It is possible to cure this failure partially with long-range corrected functionals,[23] but they introduce additional empirical parameters. An unbiased treatment of CT states is possible with wave function methods. An economic alternative to CCSD is the approximate second-order coupled cluster singles and doubles method CC2.[24] For benchmark sets that contain typical organic chromophors,[25,26] CC2 proved to be even more accurate than CCSD for singlet and triplet states that are dominated by one-electron transitions. The operation count of CC2 scales with $O(N^5)$, where N is a measure of the system size. However, if the resolution-of-the-identity (RI) or density fitting approximation is used, disk space and memory demands scale only with $O(N^3)$ and $O(N^2)$, respectively.[27] To describe singlet−triplet transitions in medium-sized molecules (up to ca. 100 atoms) that contain only light elements, the SOC-PT-based approach combined with RI-CC2 is thus an attractive computational scheme.

In the present work, we focus on SOC-induced transition moments between closed-shell singlet ground states and triplet excited states with CC2 using the perturbation approach within the framework of response theory. In contrast to earlier work at the CCSD level,[12] we fully exploit spin symmetries and derive working equations within a spin-free formalism. The theory is presented in section II. In Appendix A, we give the key steps for the derivation of the right-hand-side (RHS) vectors for the response equations. Working equations for these vectors are given in the Supporting Information (SI) section VII. In section III, we discuss the implementation with the RI approximation for the electron repulsion integrals and the use of a numerical Laplace transformation for the first-order response vectors. Results for illustrative calculations that demonstrate the accuracy and efficiency of the SOC-PT-CC2 implementation are shown in section IV.

II. THEORY

A. Perturbation Theory for Induced Singlet−Triplet Transitions. As described in the previous section, we assume that the spin−orbit interaction is small compared to the energy differences between studied states and states close by so that it is sufficient to describe it in lowest-order perturbation theory.[28] The zeroth-order ground $|0\rangle$ and excited triplet states $|f\rangle$ are pure spin states and are perturbed by the SOC operator. After expanding the states $|0(\epsilon_z)\rangle$ and $|f(\epsilon_z)\rangle$ in orders of a perturbation strength ϵ_z, the induced transition moments are in lowest order given by

$$\langle 0|X|f\rangle^{(1)} = \frac{d\langle 0(\epsilon_z)|X|f(\epsilon_z)\rangle}{d\epsilon_z} = \langle 0|X|f^{(1)}\rangle + \langle 0^{(1)}|X|f\rangle \tag{1}$$

The induced transition strength tensor becomes in lowest order

$$S_{XY}^{0f,(2)} = \langle 0|X|f\rangle^{(1)}\langle f|Y|0\rangle^{(1)} \tag{2}$$

DOI: 10.1021/acs.jctc.5b01197
J. Chem. Theory Comput. 2016, 12, 1892−1904

From the trace of the induced transition strength tensor in eq 2, one obtains the lifetime $\tau_{P,f}$ in a triplet excited state, that is, the phosphorescence lifetime

$$\frac{1}{\tau_{P,f}} = \frac{4\omega_f^3\alpha^3}{3} \sum_{i=X,Y,Z} S_{ii}^{0f} \tag{3}$$

where ω_f is the excitation energy and α the fine structure constant.

B. Derivatives of Transition Strengths in Coupled Cluster Response Theory. The induced first-order transition moments in eq 1 can be computed by response theory.[11−13] In single-reference CC theory, the wave function is given by

$$|\mathrm{CC}\rangle = \exp(T)|\mathrm{HF}\rangle \tag{4}$$

where $T = \sum_\mu t_\mu \tau_\mu$ is the cluster operator and $|\mathrm{HF}\rangle$ the Hartree−Fock (HF-SCF) determinant. For those CC models that contain single and double excitations, the cluster operator is partitioned as follows:

$$T = T_1 + T_2 = \sum_{\mu_1} t_{\mu_1}\tau_{\mu_1} + \sum_{\mu_2} t_{\mu_2}\tau_{\mu_2} \tag{5}$$

The CC ground state energy E_{CC} is determined by projecting of the Schrödinger equation onto the HF-SCF state:

$$E_{CC} = \langle \mathrm{HF}|H\exp(T)|\mathrm{HF}\rangle \tag{6}$$

For nonapproximated coupled cluster models, the equations for the amplitudes are obtained by projecting the Schrödinger equation onto an excited projection manifold

$$0 = \langle \mu|\exp(-T)H\exp(T)|\mathrm{HF}\rangle \tag{7}$$

For the CC2 model, the amplitude equations are approximated to

$$0 = \langle \mu_1|\tilde{H} + [\tilde{H}, T_2]|\mathrm{HF}\rangle = \Omega_{\mu_1} \tag{8}$$

$$0 = \langle \mu_2|\tilde{H} + [F + \epsilon\tilde{V}, T_2]|\mathrm{HF}\rangle = \Omega_{\mu_2} \tag{9}$$

where F is the Fock operator, V an external perturbation not included at the Hartree−Fock level, and ϵ the corresponding perturbation strength. μ_1 and μ_2 represent single and double excitations, respectively. The tilde on H and V in eqs 8 and 9 denotes that these operators are similarity transformed with $\exp(T_1)$ according to $\tilde{O} = \exp(-T_1)\ O\ \exp(T_1)$.

The starting point of coupled cluster response theory is the Lagrangian

$$L_{CC} = E_{CC} + \sum_\mu \bar{t}_\mu \Omega_\mu \tag{10}$$

The excitation energies ω_f are obtained by solving for either the left $\bar{E}^f$ or right eigenvectors E^f of the CC Jacobian $\mathbf{A}$ (see Table 1)

$$\mathbf{A}E^f = \omega_f E^f \tag{11}$$

$$\bar{E}^f\mathbf{A} = \bar{E}^f\omega_f \tag{12}$$

where $\mathbf{A}$ is the partial second derivative of L_{CC} with respect to the cluster amplitudes t_μ and the Lagrange multipliers $\bar{t}_\mu$. The transition strengths for an electronic excitation from the ground state $|0\rangle$ to an excited state $|f\rangle$ induced by operators X and Y are given by

Table 1. Matrices and Right-Hand Side (RHS) Vectors Needed To Compute the Induced Left and Right Transition Moments[a]

matrices	RHS vectors
$F_{\mu\nu} = \frac{\partial^2 L_{CC}}{\partial t_\mu \partial t_\nu}$	$\eta_\mu^X = \frac{\partial^2 L_{CC}}{\partial t_\mu \partial \epsilon_X}$
$G_{\mu\nu\sigma} = \frac{\partial^3 L_{CC}}{\partial t_\mu \partial t_\nu \partial t_\sigma}$	$\bar{m}^f(\omega_f) = \mathbf{F}\ E^f(\omega_f)$
$A_{\mu\nu} = \frac{\partial^2 L_{CC}}{\partial \bar{t}_\mu \partial t_\nu}$	$\xi_\mu^X = \frac{\partial^2 L_{CC}}{\partial \bar{t}_\mu \partial \epsilon_X}$
	$\bar{\xi}^X(\omega_X) = \eta^X + \mathbf{F}\ t^X(\omega_X)$
$B_{\mu\nu\sigma} = \frac{\partial^3 L_{CC}}{\partial \bar{t}_\mu \partial t_\nu \partial t_\sigma}$	
	$\xi^{f,X}(\omega_f, \omega_X) = (\mathbf{B}\ t^X(\omega_X) + \mathbf{A}^X)\ E^f(\omega_f)$
$A_{\mu\nu}^X = \frac{\partial^3 L_{CC}}{\partial \bar{t}_\mu \partial t_\nu \partial \epsilon_X}$	
	$\bar{\xi}^{f,X}(-\omega_f, \omega_X) = -\bar{E}^f(-\omega_f)(\mathbf{B}\ t^X(\omega_X) + \mathbf{A}^X)$
$F_{\mu\nu}^X = \frac{\partial^3 L_{CC}}{\partial t_\mu \partial t_\nu \partial \epsilon_X}$	

[a] X refers either to components of the electric dipole operator associated with the frequency $\omega_X = -\omega_f$ or components of the SOC operator with frequency $\omega_X = 0$.

$$S_{XY}^{0f} = \langle 0|X|f\rangle\langle f|Y|0\rangle = \frac{1}{2}(T_{0f}^X T_{f0}^Y + T_{0f}^{Y*} T_{f0}^{X*}) \tag{13}$$

The symmetrization with respect to an interchange of the operators X and Y and a simultaneous complex conjugation on RHS of eq 13 is a consequence of the non-Hermitian structure of coupled cluster theory.[29] The non-Hermitian structure of CC implies further that the left transition moments T_{0f}^X are not the adjoints of the right T_{f0}^X transition moments. They must be computed separately as

$$T_{0f}^X = \eta^X \cdot E^f + \bar{M}(\omega_f)\cdot\xi^X \tag{14}$$

$$T_{f0}^X = \bar{E}^f \cdot \xi^X \tag{15}$$

The vectors η^X and ξ^X are defined in Table 1. The Lagrange multipliers $\bar{M}^f(\omega_f)$ for the transition from $|0\rangle$ to $|f\rangle$ in eq 14 are determined by the equation[30]

$$\bar{M}^f(\omega_f)(\mathbf{A} + \omega_f\mathbf{1}) = -\bar{m}^f \tag{16}$$

The definition of the RHS vector $\bar{m}^f$ is given in Table 1. For CC wave functions, the induced transition strength tensor is given by the symmetrized product

$$S_{XY}^{0f,(2)} = \langle 0|X|f\rangle^{(1)}\langle f|Y|0\rangle^{(1)} = \frac{1}{2}\left(\frac{dT_{0f}^X}{d\epsilon_z}\frac{dT_{f0}^Y}{d\epsilon_z} + \left(\frac{dT_{0f}^Y}{d\epsilon_z}\frac{dT_{f0}^X}{d\epsilon_z}\right)^*\right) \tag{17}$$

The first derivatives of the left and right transition moments are obtained as

$$\begin{aligned}\frac{dT_{0f}^X}{d\epsilon_z} = \hat{P}^{X,z}\Bigg\{&\left[\frac{1}{2}\mathbf{G}t^X(\omega_X)t^z(\omega_z) + \mathbf{F}^X t^z(\omega_z)\right]E^f(\omega_f) \\ &+ \bar{M}^f(\omega_f)\left[\frac{1}{2}\mathbf{B}t^X(\omega_X)t^z(\omega_z) + \mathbf{A}^X t^z(\omega_z)\right] \\ &+ \bar{\xi}^X(\omega_X)\cdot E^{f,z}(\omega_f, \omega_z)\Bigg\}\end{aligned} \tag{18}$$

DOI: 10.1021/acs.jctc.5b01197
J. Chem. Theory Comput. 2016, 12, 1892−1904

$$\frac{dT^X_{f0}}{d\epsilon_z} = \bar{E}^{f,z}(-\omega_f, \omega_z)\cdot\xi^X + \bar{E}^f(-\omega_f)\mathbf{A}^X t^z(\omega_z) \tag{19}$$

For the definition of the partial derivatives of the Lagrangian **B**, $\mathbf{F}^X$, **G**, and $\mathbf{A}^X$ and the vectors $\bar{\xi}^X(\omega_X)$ and ξ^X in the above equations, see Table 1. The permutation operator $\hat{P}^{X,z}$ exchanges the components and frequencies of the dipole (X) and SOC operator (z) with each other, where the latter are associated with a frequency $\omega_z = 0$. The first derivatives of the amplitudes $t^X(\omega_X)$, left $\bar{E}^{f,X}(\omega_f,\omega_X)$, and right eigenvectors $E^{f,X}(\omega_f,\omega_X)$ are determined by the equations

$$(\mathbf{A} - \omega_X\mathbf{1})t^X(\omega_X) = -\xi^X \tag{20}$$

$$(\mathbf{A} - (\omega_X + \omega_f)\mathbf{1})E^{f,X}(\omega_f, \omega_X) = -\xi^{f,X} \tag{21}$$

$$\bar{E}^{f,X}(-\omega_f, \omega_X)(\mathbf{A} + (\omega_X - \omega_f)\mathbf{1}) = -\bar{\xi}^{f,X} \tag{22}$$

As it has already been pointed out by Christiansen and Gauss, the induced one-photon transition moments in eqs 18 and 19 differ from the left and right two-photon transition moments only in the operators (including the spin part) and frequencies.[12]

C. Spin-Free Formalism. The expressions from CC response theory in the previous section are valid for any parametrization of the cluster operator and the projection manifold. In the present work, we consider in particular closed-shell reference states. For closed-shell cases we can make use of spin symmetry to introduce singlet- and triplet-adapted excitation operators.[31] A linear independent basis for one- and two-electron excitation operators is

$${}^1\tau_{ai} = E_{ai} \tag{23}$$

$${}^1\tau_{aibj} = E_{ai}E_{bj} \text{ with } (ai) \geq (bj) \tag{24}$$

for the singlet case and

$${}^3\tau_{ai} = T_{ai} \tag{25}$$

$${}^{(+)}\tau_{aibj} = T_{ai}E_{bj} + E_{ai}T_{bj} \text{ with } a > b,\ i > j \tag{26}$$

$${}^{(-)}\tau_{aibj} = T_{ai}E_{bj} - E_{ai}T_{bj} \text{ with } (ai) > (bj) \tag{27}$$

for the triplet case, where

$$E_{ai} = a^\dagger_{a\alpha}a_{i\alpha} + a^\dagger_{a\beta}a_{i\beta} \tag{28}$$

$$T_{ai} = a^\dagger_{a\alpha}a_{i\alpha} - a^\dagger_{a\beta}a_{i\beta} \tag{29}$$

Above and in the following we follow the convention that occupied and virtual molecular orbitals (MO) are labeled with i, j, ... and a, b, ..., respectively. MOs that can be either occupied or virtual are labeled with p, q, r, s. The triplet excitation operators in eqs 25 − 27 excite from singlet-coupled configurations to the $M_S = 0$ components of triplets.

Both the Hamiltonian and the components of the dipole operator are expressed readily in a spin-free form:

$$\tilde{H} = \sum_{pq}\tilde{h}_{pq}E_{pq} + \frac{1}{2}\sum_{pqrs}\tilde{g}_{pqrs}(E_{pq}E_{rs} - \delta_{qr}E_{ps}) \tag{30}$$

$$\tilde{X} = \sum_{pq}\tilde{V}^X_{pq}E_{pq} \tag{31}$$

The effective one-electron SOC operator can be written either in Cartesian or spin-tensor form[32,33]

$$\tilde{V}_{SOC} = \frac{1}{2}\sum_{pq}(\tilde{V}^x_{pq}T^x_{pq} + \tilde{V}^y_{pq}T^y_{pq} + \tilde{V}^z_{pq}T^z_{pq}) \tag{32}$$

$$= \frac{1}{2}\sum_{M_S=-1,0,1}\sum_{pq}(-1)^{M_S}\tilde{V}^{1,-M_S}_{pq}T^{1,M_S}_{pq} \tag{33}$$

with

$$T^x_{pq} = a^\dagger_{p\alpha}a_{q\beta} + a^\dagger_{p\beta}a_{q\alpha} \tag{34}$$

$$T^y_{pq} = \frac{1}{i}(a^\dagger_{p\alpha}a_{q\beta} - a^\dagger_{p\alpha}a_{q\beta}) \tag{35}$$

$$T^z_{pq} = a^\dagger_{p\alpha}a_{q\alpha} - a^\dagger_{p\beta}a_{q\beta} \tag{36}$$

and

$$V^{1,-1}_{pq} = -V^x_{pq} - iV^y_{pq},\ V^{1,+1}_{pq} = V^x_{pq} - iV^y_{pq},\ V^{1,0}_{pq} = V^z_{pq} \tag{37}$$

From the three spin-tensor operators, only the $M_S = 0$ component $T^{1,0}_{pq} = T^z_{pq}$ does not change the M_S quantum number. For the case of a coupling between singlet and triplet states, it can be shown by employing the Wigner−Eckart theorem that only matrix elements of T^z_{pq} are necessary[9,33]

$$\langle{}^1 0|\tilde{V}^{SOC}|{}^3 f(M_S)\rangle = \frac{1}{2}\sum_{pq}\tilde{V}^{1,M_S}_{pq}\langle{}^1 0|T^{1,0}_{pq}|{}^3 f(M_S = 0)\rangle \tag{38}$$

This allows us to treat induced singlet−triplet transitions in a spin-free formalism.

The working expressions for coupled cluster are obtained by substituting the spin-free operators described above into the expressions for the partial derivatives of the Lagrangian in Table 1. Further details are given in Appendix A and in the SI section VII.

III. IMPLEMENTATION

The induced singlet−triplet transition moments have been implemented in the RI-CC2 program[27] of a development version of the TURBOMOLE package.[34] The implementation is based on the two-photon absorption (TPA) code described in ref 35 and, beyond the introduction of first-order responses of the left and right eigenvectors, mainly required an adaptation for coupling intermediates with triplet spin symmetry.

One important property of CC2 and other second-order methods is that the equations for the doubles amplitudes (9) have a simple structure, which allows for an on-the-fly computation of the amplitudes

$$t_{aibj} = \frac{1}{1 + \delta_{ij}\delta_{ab}}\frac{(ai|\tilde{1}|bj)}{\varepsilon_i - \varepsilon_a + \varepsilon_j + \varepsilon_b} \tag{39}$$

in a canonical MO basis from electron repulsion integrals in a $\mathbf{t}_1$-transformed basis:

$$(pq|\tilde{1}|rs) = \tilde{g}_{pqrs} = \sum_{\mu\nu\kappa\lambda}\Lambda^p_{\mu p}\Lambda^h_{\nu q}\Lambda^p_{\kappa r}\Lambda^h_{\lambda s}(\mu\nu|\kappa\lambda) \tag{40}$$

$$\mathbf{\Lambda}^p = \mathbf{C}(\mathbf{1} - \mathbf{t}_1^T) \tag{41}$$

$$\mathbf{\Lambda}^h = \mathbf{C}(\mathbf{1} + \mathbf{t}_1) \tag{42}$$

DOI: 10.1021/acs.jctc.5b01197
J. Chem. Theory Comput. 2016, 12, 1892−1904

In eqs 41 and 42, **C** are the MO coefficients expanded in atomic-orbital basis functions denoted with Greek letters μ,ν, ... and $\mathbf{t}_1$ is the matrix with the ground-state singles cluster amplitudes.[36] The on-the-fly generation of doubles amplitudes facilitates the implementation of effective cluster equations only for the singles, which avoids storage of four-index integrals and doubles amplitudes and saves a huge amounts of disk space and memory. This is facilitated by the RI approximation for the electron repulsion integrals:

$$(ai\tilde{|}bj) \approx \sum_{PQ} (ai\tilde{|}P)[\mathbf{V}^{-1}]_{PQ}(Q\tilde{|}bj) = \sum_{Q} \tilde{B}_{Q,\mathrm{ai}}\tilde{B}_{Q,\mathrm{bj}} \tag{43}$$

$$\tilde{B}_{Q,\mathrm{ai}} = \sum_{\mu\nu P} [\mathbf{V}^{-1/2}]_{PQ}\Lambda^{p}_{\mu a}\Lambda^{h}_{\nu i}(P|\mu\nu) \tag{44}$$

where $V_{PQ} = (P|Q)$ are two-index electron repulsion integrals for auxiliary basis functions P and Q and $(P|\mu\nu)$ three-index electron repulsion integrals. The number of three-index integrals $\tilde{B}_{Q,ai}$ is much smaller than that of four-index integrals, and they can be safely stored on disk and read when needed without introducing I/O bottlenecks. An extension to the effective eigenvalue problem and response equations was presented in ref 37 for triplet excited states in a spin-free formalism and is not repeated here. Explicit expressions for the first-order RHS vectors that involve triplet operators in eqs 20, 21, and 22 are presented in the SI section VII.

The number of necessary contractions to compute the induced left and right transition moments scales in principle with the number of transition operators n_t and the number of perturbations n_p. The formulation in eqs 18 and 19 facilitates the implementation of all contributions such that the time-determining steps depend only on either n_t or n_p. For most contributions this is achieved by formulating them as dot products of one-electron densities[35,38] with the integral matrices for the perturbation or transition operators:

$$\begin{aligned}\frac{\mathrm{d}T^{X}_{0f}}{\mathrm{d}\epsilon_z} = P^{X,z}\Big\{&\frac{1}{2}\mathbf{G}t^{X}(\omega_X)t^{z}(\omega_z)E^{f} + \frac{1}{2}\bar{M}^{f}(\omega_f)\mathbf{B}t^{X}(\omega_X)t^{z}(\omega_z)\\ &+ \mathbf{F}t^{X}(\omega_X)E^{f,z}(\omega_f,\omega_z) + \mathrm{tr}[\mathbf{D}^{F}(t^{X},E^{f})\cdot(\mathbf{V}^{z})^{T}]\\ &+ \mathrm{tr}[\mathbf{D}^{A}(\bar{M}^{f},t^{X})\cdot(\mathbf{V}^{z})^{T}] + \mathrm{tr}[\mathbf{D}^{\eta}(E^{f,X})\cdot(\mathbf{V}^{z})^{T}]\Big\}\end{aligned} \tag{45}$$

$$\frac{\mathrm{d}T^{X}_{f0}}{\mathrm{d}\epsilon_z} = \mathrm{tr}[\mathbf{D}^{\xi}(\bar{E}^{f,z})\cdot(\mathbf{V}^{X})^{T}] + \mathrm{tr}[\mathbf{D}^{A}(\bar{E}^{f},t^{z})\cdot(\mathbf{V}^{X})^{T}] \tag{46}$$

The definition of the density matrices in eqs 45 and 46 can be found in refs 35 and 38. Only one-electron densities are needed because we assume effective one-electron SOC operators as obtained by the SOMF approximation.[16,17,39] The contractions with the **G**, **B**, and **F** matrices can be reformulated following similar lines by means of generalized derivative Fock matrices and three-index intermediates that originate from the RI approximation as shown in refs 35 and 40.

In the doubles parts of the RHS vectors for the response eqs 20−22 appears the doubles part of at least one undifferentiated amplitude or eigenvector. In a previous work,[35] the orbital energy denominator $x = \varepsilon_a - \varepsilon_i + \varepsilon_b - \varepsilon_j$ of the zeroth-order doubles was factorized by using the numerical Laplace transformation[41]

$$\frac{1}{x} = \int_0^\infty \exp(-xt)\mathrm{d}t \approx \sum_{\alpha=1}^{n_\alpha} \omega_\alpha \exp(-xt_\alpha) \tag{47}$$

with quadrature weights ω_α and grid points t_α. In combination with the RI approximation, this reformulation leads to two- and three-index intermediates, which can be precomputed so that both RHS and solution vectors can be evaluated without storing quantities with four orbital indices. As an example, we show explicit expression for the RHS vector of the first-order amplitudes

$$\xi^{X}_{aibj} = \hat{P}^{ij}_{ab}\sum_{\alpha,Q}\omega_\alpha K^{\alpha}_{Qai}\bar{K}^{\alpha,X}_{Qbj} \tag{48}$$

$$K^{\alpha}_{Qai} = \tilde{B}_{Qai}\exp((\varepsilon_i - \varepsilon_a)t_\alpha) \tag{49}$$

$$\bar{K}^{\alpha,X}_{Qai} = \sum_c K^{\alpha}_{Qci}V^{X}_{ac} - \sum_k K^{\alpha}_{Qak}V^{X}_{ki} \tag{50}$$

In the equation above, $\hat{P}^{ij}_{ab}$ is defined by $\hat{P}^{ij}_{ab}f_{aibj} = f_{aibj} + f_{bjai}$. In contrast to the TPA implementation of ref 35, we use in the current work the Laplace transformation only to evaluate the doubles parts of derivatives of amplitudes and eigenvectors during the construction of one-electron density matrices, but no longer to compute the RHS vectors for response equations. This improves the convergence with the number of quadrature points as the contributions from the affected densities to the final results are small. The convergence of the phosphorescence lifetimes with the thresholds for the linear response equations and the numerical Laplace transformation is investigated in section IV B.

The coupling between the singlet and triplet states is described by the SOMF operator[16,17] with matrix elements

$$\begin{aligned}V^{z,\mathrm{SOMF}}_{\mu\nu} = (\mu|h^{z}|\nu) + \sum_{\kappa\lambda} D_{\kappa\lambda}\Big\{&(\kappa\lambda|g^{z}|\mu\nu) - \frac{3}{2}(\mu\kappa|g^{z}|\lambda\nu)\\ &+ \frac{3}{2}(\lambda\nu|g^{z}|\mu\kappa)\Big\}\end{aligned} \tag{51}$$

$$h^{z} = \frac{1}{2c^2}\sum_K \frac{Z_k[\mathbf{r}_K\times\mathbf{p}]_z}{r^3_K} \tag{52}$$

$$g^{z} = \frac{1}{2c^2}\frac{[\mathbf{r}_{12}\times\mathbf{p}_2]_z}{r^3_{12}} \tag{53}$$

that include the one-electron and an effective two-electron contribution together with the spin-averaged HF-SCF density matrix $D_{\kappa\lambda}$. Note that z in eqs 51−53 is one component of the SOMF operator, but all three components are needed to compute phosphorescence lifetimes. The one- and two-electron spin−orbit integrals, that is, $(\mu|\, h^z\,|\nu)$ and $(\mu\,\nu\,|\,g^z\,|\,\kappa\,\lambda)$, can be expressed as conventional integrals with differentiated basis functions.[9] A derivation for the spin−orbit two-electron integrals is presented in the SI section VII.

It was shown by numerous numerical investigations that mean-field SOC operators yield phosphorescence lifetimes that are very close to those obtained with the full BP operator.[12,42,43] In our implementation, the SOMF integrals are apart from standard integral screening computed without further approximations and are, concerning the two-electron part, contracted directly with the density matrix. Alternatively, the SOMF matrices can be read from a file generated by an

DOI: 10.1021/acs.jctc.5b01197
J. Chem. Theory Comput. 2016, 12, 1892−1904

external program that can be used to import SOMF matrices computed with the REL module of the ORCA package.[18,39]

IV. ILLUSTRATIVE CALCULATIONS

A. General Computational Details. All 1C HF-SCF calculations were performed with the dscf program[44] of the TURBOMOLE package.[34] Calculations that include SR effects from the spin-free X2C Hamiltonian[45] were also carried out with dscf. For these 1C HF-SCF calculations, we made use of point group symmetry. Some results were obtained with SOMF matrices computed with the REL module[18] of the ORCA package[39] release 3.0.2, which will be noted explicitly below. In these calculations, the effective operator consists of (1) the one-electron part of the BP operator, (2) the Coulomb term computed with the RI approximation, (3) the exchange terms computed via a one-center approximation, and (4) a DFT local correlation term.[46]

All two-component X2C-HF-SCF and X2C-CC2 calculations were carried out with the ridft[45,47] and ricc2 programs, respectively,[15,27] of TURBOMOLE V7.0.[48] X2C-HF-SCF calculations made use of the RI approximation for both the Coulomb and exchange two-electron integrals (RI-JK). No point group symmetry was used for these calculations due to technical limitations. Point charge nuclei were used throughout. Neither the Gaunt nor the Breit term were included in the two-electron interaction part of the Dirac−Hamiltonian at both the SCF and the correlated level.

In our calculations, we used the cc-pVTZ,[49] aug-cc-pVDZ, aug-cc-pVTZ,[50] def2-TZVPP, and def2-QZVPP[51] orbital basis sets. For all CC2 calculations, we used auxiliary basis sets from refs 52 and 53, optimized for the corresponding orbital basis sets. X2C-HF-SCF calculations were performed with auxiliary RI-JK basis sets from ref 54. In all CC2 calculations, both 1C and 2C, we kept the core electrons frozen.

DFT geometry optimizations were done with the D3 dispersion-corrected[55] hybrid functional PBE0[56]-D3.

B. Accuracy of the Numerical Laplace Transformation. To determine balanced convergence thresholds for the response equations T_{LRE} and the numerical Laplace transformation T_{LAP}, we studied the convergence of the relative errors in the phosphorescence lifetime $\tau_{P,f}$ with T_{LRE} and T_{LAP} for the 1 $^3B_2$ and 2 ^3A_u state in thiophene and pyrazine, respectively. For these calculations we used SOC integrals from the ORCA package. In all other investigations SOC integrals from our own SOMF implementation were used. Among the lowest excited triplet states in these two molecules, the 1 $^3B_2$ and 2 ^3A_u state feature the shortest lifetimes. The quadrature parameters ω_α and t_α are obtained from the least-squares minimization[57] of

$$F^{\mathrm{LAP}} = \int_{x_{\min}}^{x_{\max}} \left(\frac{1}{x} - \sum_{\alpha=1}^{n_\alpha} \omega_\alpha \exp(-t_\alpha x) \right)^2 \mathrm{d}x \tag{54}$$

The number of quadrature points n_α is increased until $\sqrt{F^{\mathrm{LAP}}} \leq T_{\mathrm{LAP}}$. The dependence of relative errors $\Delta_{\mathrm{rel}}\ \tau_{P,f}$ in τ_P on T_{LRE} and n_α is shown in Figure 1a,b for thiophene and pyrazine, respectively. The calculations for the 1 $^3B_2$ state of thiophene were done with the cc-pVTZ basis. We find that for this example the relative errors follow roughly the relation $\Delta_{\mathrm{rel}}\ \tau_{P,f} \approx 0.1\ T_{\mathrm{LRE}} + 0.01\ T_{\mathrm{LAP}}$. The lifetimes in the 2 ^3A_u state of pyrazine were calculated in the aug-cc-pVTZ basis. For the more diffuse orbital basis we observe a slightly slower

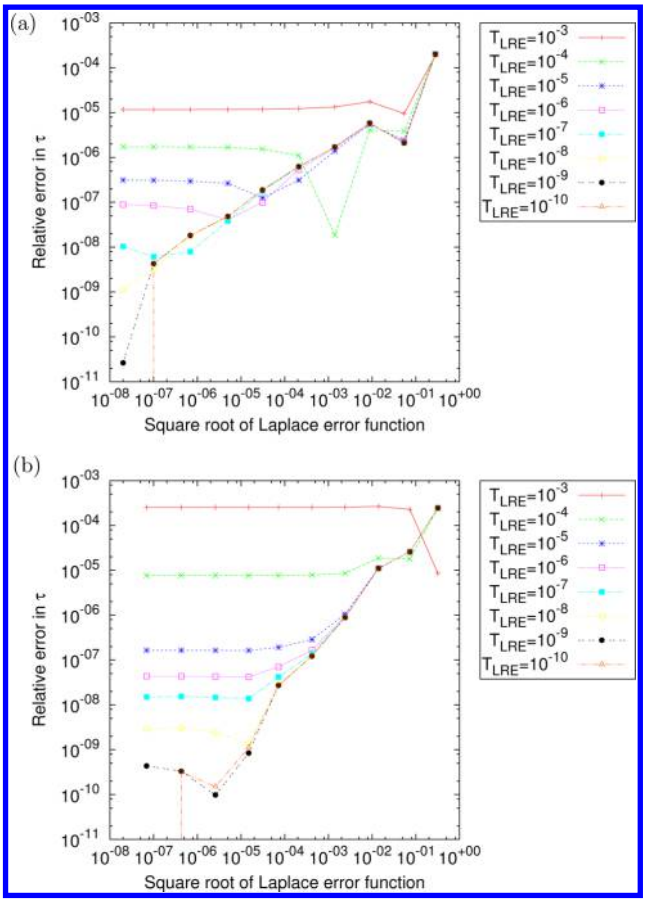


Figure 1. The cc-pVTZ basis set was used in (a) and aug-cc-pVTZ in (b).

convergence with T_{LRE}. The relative error $\Delta_{\mathrm{rel}}\ \tau_{P,f}$ can for this case be approximated by $\Delta_{\mathrm{rel}}\ \tau_{P,f} \approx T_{\mathrm{LRE}} + 0.01\ T_{\mathrm{LAP}}$ and is in the regime where T_{LRE} is roughly a factor of 10 larger than with the cc-pVTZ basis. From the two numerical examples, we see that an accuracy of $\Delta_{\mathrm{rel}}\ \tau_{P,f} = 10^{-4}$ in the lifetimes, which is more than sufficient for CC2, is achieved with $T_{\mathrm{LRE}} = 10^{-4}$ and $T_{\mathrm{LAP}} = 10^{-2}$. For applications reported in the following, we used these thresholds.

C. Validation of Perturbation Theory. To assess the applicability of SOC-PT, we computed excitation energies ω_f and phosphorescence lifetimes $\tau_{P,f}$ for the halogen hydrides HF, HCl, and HBr with both PT and X2C at the CC2 level. Experimental bond distances were taken from the NIST database[58] for the most abundant isotopes and are 0.9168, 1.2746, and 1.4144 Å for HF, HCl, and HBr, respectively. The results for the two lowest $^3\Sigma^+$ and $^3\Pi$ states computed with the aug-cc-pVTZ basis set are listed in Table 2. In general, the degeneracy between the three components of triplet states is lifted when employing the Dirac−Coulomb Hamiltonian for X2C calculations. To compare PT with X2C results, averaged values for X2C excitation energies and lifetimes are shown Table 2. 1C and 2C states can be related in first-order PT if the direct product of irreducible representations (*irrep*) of the 1C state with a component of the SOC operator contains the *irrep* of the 2C state. In the case of halogen hydrides (point group $C_{\infty v}$), Σ^- and Π are related to $^3\Sigma^+$; Σ^+, Σ^-, Π, and Δ are related to $^3\Pi$. For lifetimes, it is assumed that all three components of the triplet state in a 2C calculation are populated equally

DOI: 10.1021/acs.jctc.5b01197
J. Chem. Theory Comput. 2016, 12, 1892−1904

Table 2. Excitation Energies ω_f (eV) and Phosphorescence Lifetimes $\tau_{P,f}$ (ms) of the Two Lowest Excited $^3\Sigma^+$ and $^3\Pi$ States for Halogen Hydrides[a]

	NR			SR			X2C	
		1e-SOC	SOMF		1e-SOC	SOMF		
state	ω_f	$\tau_{P,f}$	$\tau_{P,f}$	ω_f	$\tau_{P,f}$	$\tau_{P,f}$	ω_f	$\tau_{P,f}$
				HF				
$1\ ^3\Pi$	9.61	1.1×10^{-3}	1.4×10^{-3}	9.60	1.1×10^{-3}	1.4×10^{-3}	9.61	1.8×10^{-3}
$1\ ^3\Sigma^+$	13.26	1.8×10^{-1}	2.3×10^{-1}	13.25	1.8×10^{-1}	2.3×10^{-1}	13.26	2.8×10^{-1}
$2\ ^3\Pi$	12.95	3.7×10^{-4}	4.6×10^{-4}	12.94	3.7×10^{-4}	4.6×10^{-4}	12.93	4.4×10^{-4}
$2\ ^3\Sigma^+$	13.57	7.0×10^{-1}	8.9×10^{-1}	13.56	6.8×10^{-1}	8.7×10^{-1}	13.56	$2.4 \times 10^{+0}$
				HCl				
$1\ ^3\Pi$	7.46	1.7×10^{-3}	1.9×10^{-3}	7.44	1.7×10^{-3}	1.9×10^{-3}	7.44	2.4×10^{-3}
$1\ ^3\Sigma^+$	10.29	1.1×10^{-2}	1.2×10^{-2}	10.28	9.9×10^{-3}	1.1×10^{-2}	10.28	1.7×10^{-2}
$2\ ^3\Pi$	9.50	3.2×10^{-4}	3.6×10^{-4}	9.50	3.2×10^{-4}	3.6×10^{-4}	9.66	4.7×10^{-4}
$2\ ^3\Sigma^+$	10.43	9.6×10^{-3}	1.1×10^{-2}	10.42	9.2×10^{-3}	1.0×10^{-2}	10.42	1.2×10^{-2}
				HBr				
$1\ ^3\Pi$	6.46	2.6×10^{-4}	2.8×10^{-4}	6.42	2.5×10^{-4}	2.6×10^{-4}	6.49	5.1×10^{-4}
$1\ ^3\Sigma^+$	9.07	1.2×10^{-4}	1.2×10^{-4}	9.03	6.7×10^{-5}	7.0×10^{-5}	9.05	1.2×10^{-4}
$2\ ^3\Pi$	8.41	1.7×10^{-5}	1.8×10^{-5}	8.43	1.9×10^{-5}	2.0×10^{-5}	8.42	4.4×10^{-5}
$2\ ^3\Sigma^+$	9.39	7.8×10^{-3}	8.2×10^{-3}	9.38	4.9×10^{-3}	5.2×10^{-3}	9.29	6.6×10^{-4}

[a] ω_f and $\tau_{P,f}$ were calculated with the RI-CC2/aug-cc-pVTZ method by using either the exact two-component (X2C) Hamiltonian or spin-orbit coupling perturbation theory (SOC-PT) with (SR) or without (NR) scalar-relativistic effects from the spin-free X2C Hamiltonian.

$$\langle \tau_{P,f} \rangle = 3(\tau_{P,f,1}^{-1} + \tau_{P,f,2}^{-1} + \tau_{P,f,3}^{-1})^{-1} \quad (55)$$

However, only Σ^+ and Π contribute to $\langle \tau_{P,f} \rangle$ for point group symmetry reasons.

For the RI-CC2/aug-cc-pVTZ method, the lifetimes $\tau_{P,f}$ obtained with SOC-PT and X2C differ at most by a factor of 2.8, 2.1, and 9.3 for the halogen hydrides HF, HCl, and HBr, respectively (Table 2). At the same time the deviation for the excitation energies $\Delta\omega_f$ increases from 13 to 21 and 52 meV for HF, HCl, and HBr, respectively. The differences in the excitation energies are much lower if the SR contribution are included in the 1C calculations (i.e., 3, 3, and 38 meV for HF, HCl, and HBr, respectively). However, we observe no significant improvement for the lifetimes.

The phosphorescence lifetimes in the $2\ ^3\Sigma^+$ state of HBr give the largest deviations between the (SR-)SOC-PT and X2C calculations. In the 2C calculation, the 7 Π state is only 84 meV above 6 Π (cf. Figure 2). The 6 Π and 7 Π states of the 2C calculation correlate with the $3\ ^3\Pi$ and $2\ ^3\Sigma^+$, respectively, in the 1C calculation where $\tau_{P,f}$ differs by 686% (not shown for the $3\ ^3\Pi$ state) and −96%. Thus, the SOC-PT approach to phosphorescence lifetimes is not valid if two or more 2C states of the same point group symmetry are close in energy and couple to different 1C states. This usually happens for higher excited states in molecules with heavy elements where the splitting in a 2C calculation due to SOC can be larger than the energy gap between the 1C states.

Typical target applications of SOC-PT approaches are $T_1 \rightarrow S_0$ transition rates. For this particular transition, the relative deviations to X2C are in the range of −23% and −48% for the lightest (HF) and heaviest molecule (HBr) that we have investigated. Considering the methodological error and the computational demands of the CC2 method, the agreement of SOC-PT with X2C lifetimes is encouraging. Furthermore, the deviations of SOC-PT and X2C lifetimes are for CC2 in the same ballpark as at the TDSCF level. For formaldehyde (H_2CX with X = O) and its higher homologues (X = S,Se, and Te), Jansson et al.[43] reported lifetimes for T_1 obtained with SOC-PT and 4C methods. They found deviations between 21% (X = O) and 9% (X = Te).

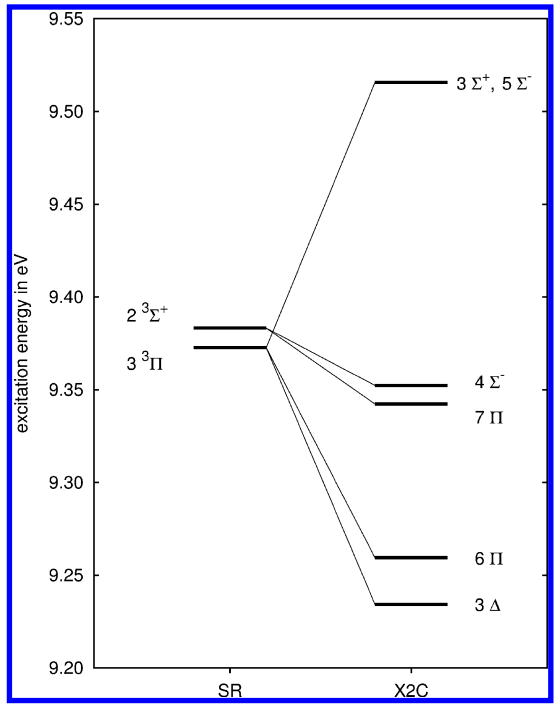


Figure 2. CC2/aug-cc-pVTZ excitations energies of HBr with either the exact 2C (X2C) Hamiltonian or a 1C method that accounts for scalar-relativistic (SR) effects from the spin-free X2C Hamiltonian.

D. Efficiency of Perturbation Theory. To assess the efficiency of the SOC-PT-CC2 approach, we computed the lifetime in the $1\ ^3B_{3u}$ state of pyrazine with SOC-PT and X2C in the aug-cc-pVTZ basis. The structure of pyrazine was taken from the benchmark set of Schreiber et al.[25] The timings for the key steps are depicted in Figure 3. The calculations were carried out on a node with a single Intel Xeon CPU E5345 with a clock rate of 2.33 GHz. Because point group symmetry can currently not be exploited for the X2C-CC2 implementation, both

DOI: 10.1021/acs.jctc.5b01197
J. Chem. Theory Comput. 2016, 12, 1892−1904

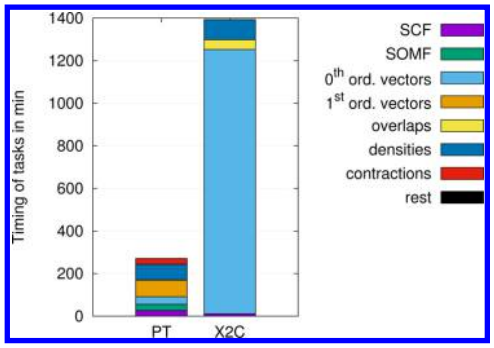


Figure 3. Timings in minutes for computing the lifetime in the 1 $^3B_{3u}$ state of pyrazine with RI-CC2/aug-cc-pVTZ. Spin−orbit coupling perturbation theory (SOC-PT) and the exact two-component (X2C) approach were applied.

calculations were done without point group symmetry for better comparison.

As shown in Figure 3, both the HF-SCF procedure and SOMF integral evaluation contribute almost equally to the total wall time of the SOC-PT calculation, 10% for the current example. This is related to the small size of pyrazine and the diffuse functions in the aug-cc-pVTZ basis set, which deteriorate the integral screening. For more extended systems, which are in the focus of the method, these two steps will contribute only little to the overall wall time of a CC2 calculation. The X2C-SCF was for technical reasons performed with the RI-JK approximation. With the aug-cc-pVTZ basis the X2C-SCF with RI-JK is for pyrazine 2.5 times faster than the 1C-SCF calculation without RI-JK.

The main contribution to the total wall time comes from the $O(N^5)$ scaling CC2 calculation. For X2C, we only need to solve in total 5 zeroth-order equations for t, $\bar{t}$, E^f, $\bar{E}^f$, and $\bar{M}^f$, where only 3 equations depend on the excited state f. For SOC-PT, 15 additional response equations have to be solved, 3 for each vector $t^X(-\omega_f)$, $t^Z(0)$, $E^{f,X}(\omega_f-\omega_f)$, $E^{f,Z}(\omega_f, 0)$, and $\bar{E}^{f,Z}(-\omega_f 0)$ (cf. eqs 18 and 19). From those 15 additional equations, 12 depend on the excited state f. This means that, compared to X2C, we solve for SOC-PT 4 times as many (state-dependent) equations. Despite this fact, the solution of all cluster and response equations is for SOC-PT-CC2, 10 times faster than for X2C-CC2.

Concerning the number of required one-electron densities, the difference between SOC-PT and X2C is even more distinct. For X2C-CC2, only three densities, that is, $\mathbf{D}^\eta(E^f)$, $\mathbf{D}^\xi(\bar{M}^f)$, and $\mathbf{D}^\xi(\bar{E}^f)$, are needed for the left and right transition moments (cf. eqs 14 and 15). For SOC-PT-CC2, 24 additional densities, that is, 6 $\mathbf{D}^\eta$, 3 $\mathbf{D}^\xi$, 9 $\mathbf{D}^A$, and 6 $\mathbf{D}^F$, are needed altogether to compute the SOC-induced left and right transition moments (cf. eqs 45 and 46). Although 7 times more densities have to be calculated for SOC-PT, their computation is in the pyrazine example still 22% faster than for X2C. Additionally, the SOC-PT calculation requires the evaluation of additional contractions of response vectors with partial derivatives of the Lagrangian, which are not formulated in terms of densities. However, they contribute only little with about 10% to the total wall time.

Despite the larger number of response equations, densities, and contractions a SOC-PT-CC2 calculation for phosphorescence lifetimes is roughly 5 times faster than with X2C-CC2. This is related to the spin-free formalism, which can be used for SOC-PT, while X2C-CC2 uses complex two-component spinors. This leads for the $O(N^5)$ -scaling steps in CC2 to a factor of 64 in the operation counts for the two approaches (if no time-reversal symmetry is exploited at the 2C level). To compute high-temperature average lifetimes with X2C, the transition rates for all three components of a triplet state are required. For the high-temperature average lifetime calculation of pyrazine, the SOC-PT-based RI-CC2 implementation was eventually 12 times faster than the corresponding X2C calculation.

E. Application to Small Organic Phosphorescent Emitters. The target applications of SOC-PT-CC2 are phosphorescence lifetimes of closed-shell organic dyes like thioketones, for which large phosphorescence quantum yields have been observed experimentally.[59] Lifetimes in the lowest triplet state of the thioketones dithiosuccinimide and 4*H*-pyran-4-thione were recently calculated with multireference SOCI[60] (MRSOCI) and X2C-CC2[15] methods. The oscillator strengths of each component of the lowest triplet state and high-temperature average phosphorescence lifetimes are compiled in Tables 3 and 4 for dithiosuccinimide and 4*H*-pyran-4-thione, respectively. We have calculated oscillator strengths and lifetimes with SOC-PT-CC2 for the same excited state equilibrium structures that were used for the X2C-CC2 calculation in ref 15 from a geometry optimization[61] at the CC2/def2-TZVPP level including SR effects from the spin-free X2C Hamiltonian.

Table 3. Oscillator Strengths (a.u.) of Each Component of the Lowest Triplet State 1 $^3B_1$ in Dithiosuccinimide and the High-Temperature Average Lifetime (ms)[a]

method	MRSOCI[bc]	X2C-CC2[c]	SOC-PT-CC2	SOC-PT-CC2
symmetry	C_{2v}	C_2	C_2	C_1
		oscillator strength		
1 $^3B_1(A_2)$	1.3×10^{-9}	4.6×10^{-9}	2.9×10^{-8}	2.3×10^{-5}
1 $^3B_1(B_2)$	2.1×10^{-5}	2.4×10^{-5}	1.7×10^{-5}	2.7×10^{-6}
1 $^3B_1(A_1)$	3.6×10^{-6}	3.5×10^{-6}	2.5×10^{-6}	7.7×10^{-6}
		lifetime		
$\langle 1\ ^3B_1\rangle$	0.52	0.38	0.18	0.18

[a]Experimental value is 0.2 ms.[60]. [b]Results taken from ref 60. [c]Results taken from ref 15.

Table 4. Oscillator Strengths (a.u.) of Each Component of the Lowest Triplet State 1 $^3A_2$ in 4*H*-Pyran-4-thione and the High-Temperature Average Lifetime (ms)[a]

method	MRSOCI[bc]	X2C-CC2[c]	SOC-PT-CC2
symmetry	C_{2v}	C_{2v}	C_{2v}
		oscillator strength	
1 $^3A_2(B_1)$	5.1×10^{-8}	1.8×10^{-8}	1.2×10^{-8}
1 $^3A_2(B_2)$	2.6×10^{-7}	1.4×10^{-7}	1.0×10^{-7}
1 $^3A_2(A_1)$	6.5×10^{-5}	8.0×10^{-5}	5.6×10^{-5}
		lifetime	
$\langle 1\ ^3A_2\rangle$	0.33	0.21	0.097

[a]Experimental value is 0.1 ms[60]. [b]Results taken from ref 60. [c]Results taken from ref 15.

For dithiosuccinimide, an analysis of the harmonic vibrational frequencies reveals that the equilibrium structure (cf. SI section VII) obtained for the 1 ^3B state under C_2 symmetry constraints is a saddle point. A true minimum structure (cf. SI section VII) for the lowest triplet excited state 1 ^3A has no

DOI: 10.1021/acs.jctc.5b01197
J. Chem. Theory Comput. 2016, 12, 1892−1904

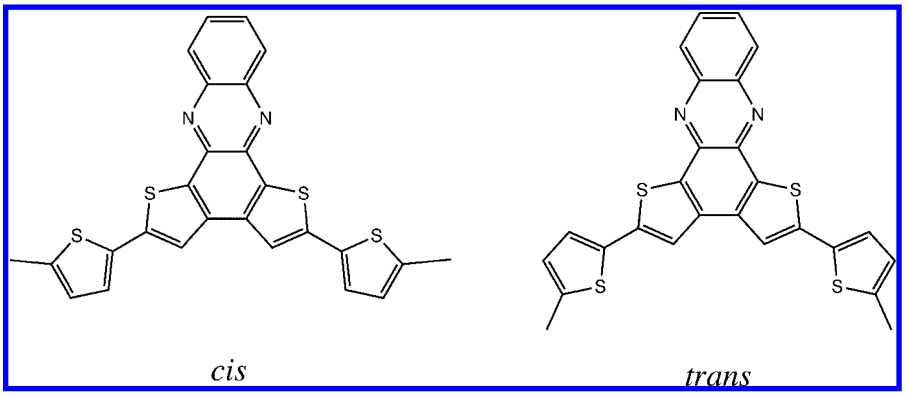


Figure 4. Lewis structures of the *all-cis* and *all-trans* conformer of phosphorescence emitter **1**.

symmetry elements and is 7.6 kJ/mol lower in energy than the saddle point with C_2 symmetry used in ref 15.

As shown in the first three columns of Table 3, the oscillator strengths for the $T_1 \rightarrow S_0$ transitions are in the SOC-PT-CC2 calculation for the two dominant of the three components not more than 30% smaller than the respective MRSOCI and X2C-CC2 results if the C_{2v} and C_2 symmetric structures are used. For the C_1 structure, all three components of the $T_1 \rightarrow S_0$ transition have sizable oscillator strengths and contribute to the lifetime of T_1. Nevertheless, the phosphorescence lifetime for T_1 obtained with SOC-PT-CC2 is almost identical (0.18 ms) for the C_2 and C_1 structures due to the smaller transition energy of 1.93 eV of the C_1 structure compared to 2.58 eV at the saddle point with C_2 symmetry. The lifetimes for the T_1 state of dithiosuccineimide obtained with MRSOCI, X2C-CC2, and SOC-PT-CC2 agree reasonably well with the experimental result of 0.2 ms. The SOC-PT-CC2 result shows the best agreement.

For 4*H*-pyran-4-thione, a force constant calculation confirms that the structure with C_{2v} symmetry obtained in ref 15 for the $1\ ^3A_2$ state is a minimum on the CC2/def2-TZVPP potential energy surface for T_1, which included SR contributions from the spin-free X2C Hamiltonian. Again, all components of the $T_1 \rightarrow S_0$ oscillator strengths are in the same order of magnitude for all three computational methods. SOC-PT-CC2 gives oscillator strengths that are slightly smaller that those obtained with MRSOCI and X2C-CC2. Though the lifetimes for the $1\ ^3A_2$ state computed with all three methods are in good agreement with the experimental value of 0.1 ms, the SOC-PT-CC2 result is with 0.097 ms closest to experiment.

F. Application to Metal-Free OLEDs. Recently, Chaudhuri et al.[62] proposed two purely organic molecules as possible phosphorescent emitters for OLED devices. For one of them, structure **1** in Figure 4, we have calculated phosphorescence lifetimes with SOC-PT-CC2. For the calculations, we have replaced all pentyl by methyl groups. Two possible conformers for **1** were investigated (cf. Figure 4). For the *all-cis* conformer, sulfur atoms of adjacent thiophene units are on the same side of the molecule, for the *all-trans* conformer they are on opposite sides. For both conformers, we have optimized the ground-state structure with dispersion-corrected hybrid DFT (PBE0+D3/def2-QZVPP) including SR effects from the spin-free X2C Hamiltonian. Both conformers feature a twisted C_2 symmetric structure (cf. SI section VII). The *all-trans* conformer has a 7.7 kJ/mol lower energy than the *all-cis* conformer. The dihedral angles between two adjacent sulfur atoms ∠ (S−C−C−S) are 25.8° and 12.3° for the *all-cis* and *all-trans* conformer, respectively. The same dihedral angles are 27.6° and 20.2° if the ground-state geometry is optimized at the second-order Møller−Plesset perturbation theory level (MP2/def2-QZVPP) with SR contributions from the spin-free X2C Hamiltonian (cf. SI section VII). Also for the MP2 equilibrium geometries, the *all-trans* conformer is more stable than the *all-cis* conformer by 4.1 kJ/mol.

For both conformers, we also determined the equilibrium geometries of the lowest excited triplet state $1\ ^3B$ at the CC2 level with the aug-cc-pVDZ and aug-cc-pVTZ basis set. Again, the SR part of the X2C Hamiltonian was included. In contrast to the ground state, the equilibrium structure in the lowest excited triplet state $1\ ^3B_2$ has C_{2v} symmetry (cf. SI section VII). For the *all-trans* conformer, the most dominant occupied and virtual natural transition orbital[63] for the $T_1 \rightarrow S_0$ transition is shown in Figure 5. The emission energies and lifetimes of $1\ ^3B_2$ are compiled in Table 5 for the two conformers. The emission energies of both conformers differ by less than 0.06 eV from the experimental transition energy at the band maximum even though vibrational corrections were not included. The SOC-

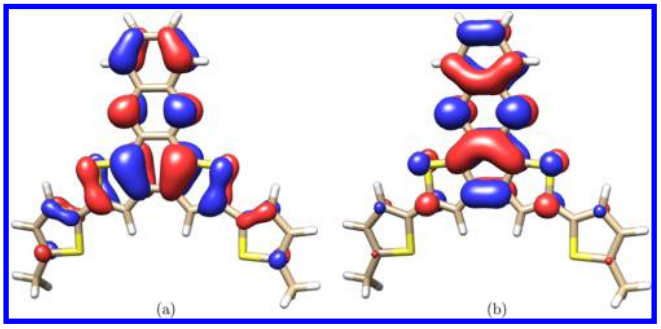


Figure 5. Most dominant occupied (a) and virtual (b) natural transition orbital of the *all-trans* conformer of phosphorescence emitter **1**.

Table 5. Emission Energy ω (eV) and Lifetime $\tau_{P,f}$ (ms) of the $1\ ^3B_2$ State of Phosphorescence Emitter 1 for the *all-cis* and *all-trans* Conformer Using the aug-cc-pVDZ (ADZ) and aug-cc-pVTZ (ATZ) Basis Set

conformer	basis set	ω	$\tau_{P,f}$
all-cis	ADZ	1.80	1.9×10^5
all-trans	ADZ	1.77	1.4×10^3
all-trans	ATZ	1.80	1.3×10^5
experiment		1.83	1.1×10^1

DOI: 10.1021/acs.jctc.5b01197
J. Chem. Theory Comput. 2016, 12, 1892−1904

PT-CC2 results also confirm the experimental finding that the T_1 state for these molecules has a rather long lifetime. The computed pure electronic gas phase results for the phosphorescence lifetimes $\tau_{P,f}$ are in the order of 10^3−10^5 ms. At these time scales, other relaxation mechanisms dominate and prevent a quantitative comparison with the experimentally observed lifetime for T_1.

The calculations with the aug-cc-pVTZ basis set comprised 1856 orbital and 4292 auxiliary basis functions and 154 electrons were correlated in the CC2 calculations. For the SOC-PT-CC2 calculations, the full symmetry of the C_{2v} point group was exploited. With a shared-memory parallelization, the calculation took on 8 cores of an Intel Xeon CPU E5430 with a clock rate of 2.66 GHz 7 days and 3 h. Only 8% of the total wall time were spent on the evaluation of the SOMF integrals, though a basis set was used that contains diffuse basis functions. Among the reported calculations in the literature, this is to our best knowledge the largest phosphorescence calculation with a correlated wave function method.

V. CONCLUSIONS

We reported the first formulation and implementation of any coupled cluster response method for transition moments between closed-shell singlet ground states and triplet excited states in a spin-free formalism. To compute the electronic transition moments for the "spin-forbidden" transitions from triplet excited states to the ground state, we treat spin−orbit coupling as perturbation.[11−13]

In our implementation, we employed the SOMF approximation to the Breit−Pauli operator, where the mean field two-electron contribution is computed in an integral-direct way from the Hartree−Fock density. Even with diffuse basis sets, the SOMF integral computation does not contribute more than 10% to the total wall time of phosphorescence calculations performed in this work. For the largest molecules considered here, only 8% of the total wall time were spent on the SOMF integral evaluation. The RI-CC2 implementation of the SOC-induced transition moments is based on an earlier reported implementation for two-photon matrix elements[35] but uses the numerical Laplace transformation only for one-electron density matrices that involve derivatives of the cluster amplitude or eigenvectors. This allows us to use less Laplace quadrature points while the same accuracy is achieved. For RI-CC2 the perturbative treatment of spin−orbit coupling is roughly 12 times faster than a two-component relativistic calculation[15] if high-temperature averages of phosphorescence lifetimes are computed.

With respect to accuracy, we could show that for the lowest triplet states in halogen hydrides, SOC-PT-CC2 gives lifetimes that differ typically by not more than 50% from those obtained with X2C-CC2. Only for higher nearly degenerate states in molecules with heavy elements like bromine, the perturbative treatment is a poor approximation because the spin−orbit corrections to the excitation energies approach the same order of magnitude as the energy differences between the electronic states in a one-component calculation. SOC-PT-CC2 results for the lifetimes of the lowest triplet states in two small organic thioketones agree well with those obtained with MRSOCI[60] and X2C-CC2[15] and differ from the experimental values only insignificantly. The applicability of SOC-PT-CC2 to large molecules is demonstrated at the example of a recently proposed phosphorescence emitter[62] for OLED devices with 154 correlated electrons and more than 1800 basis functions in the aug-cc-pVTZ basis. The CC2/aug-cc-pVTZ emission energy from the lowest triplet state deviates by less than 0.03 eV from the experimental transition energy at the band maximum. The SOC-PT-CC2 results predict in agreement with the experimental results a low transition rate for the $T_1 \rightarrow S_0$ relaxation. However, the lifetime is too long to allow a quantitative comparison of the experimental results with the pure electronic transition rates obtained from a gas phase calculation.

APPENDIX A: DERIVATION OF THE FIRST-ORDER RHS VECTORS THAT INVOLVE TRIPLET OPERATORS

1. Commutators of the Hamiltonian and Perturbation Operators. Explicit expressions for the intermediates and response vectors to compute the induced left and right transition moments are derived from the second-quantization expressions in Table 1. This involves the Baker−Campbell−Hausdorff expansion of the operator O

$$\exp(-T)O\exp(T) = O + [O, T] + \frac{1}{2}[[O, T], T] + \ldots \tag{A1}$$

which is in our case either the T_1-transformed Hamiltonian $\tilde{H}$ or one-electron perturbation operator ($\tilde{X}$ or $\tilde{V}^z_{SOC}$). We follow the strategy presented in ref 32 and reduce those expressions in terms of nested commutators of the Hamiltonian (or perturbation operator) and single-excitation operators E_{ai} and T_{ai}. All required commutators for the Hamiltonian are compiled in Table 6. Commutators for the singlet one-electron

Table 6. Commutators of the Operators $\hat{H}$ and $\hat{V}^z_{SOC}$ with One-Electron Singlet and Triplet Excitation Operators

$[\hat{H},T_{ai}]$	=	$\hat{h}_{pa}\,T_{pi} - \hat{h}_{ip}\,T_{ap} + g_{pqra}\,\tilde{\tau}_{pqri} - g_{pqir}\,\tilde{\tau}_{pqar}$
$[[\hat{H},E_{ai}],T_{bj}]$	=	$-P_{ai,bj}\{\hat{h}_{ja}\,T_{bi} + g_{pqja}\,\tilde{\tau}_{pqbi}\} - g_{jqra}\,\tilde{\tau}_{ribq} - g_{iqrb}\,\tilde{\tau}_{aqrj} + g_{pbra}\,\tilde{\tau}_{ripj} + g_{iqjs}\,\tilde{\tau}_{aqbs}$
$[[\hat{H},T_{ai}],E_{bj}]$	=	$-P_{ai,bj}\{\hat{h}_{ja}\,T_{bi} + g_{pqja}\,\tilde{\tau}'_{bipq}\} - g_{jqra}\,\tilde{\tau}'_{ribq} - g_{iqrb}\,\tilde{\tau}'_{aqrj} + g_{pbra}\,\tilde{\tau}'_{ripj} + g_{iqjs}\,\tilde{\tau}'_{aqbs}$
$[[\hat{H},T_{ai}],T_{bj}]$	=	$-P_{ai,bj}\{\hat{h}_{ja}\,E_{bi} + g_{pqja}\,e_{bipq} + g_{jqra}\,\tau_{ribq}\} + g_{pbra}\,\tau_{pjri} + g_{jqis}\,\tau_{bqas}$
$[[[\hat{H},T_{ai}],E_{bj}],E_{ck}]$	=	$+ P_{bj,ck}\{g_{kpja}\,\tilde{\tau}'_{bicp} - g_{pcja}\,\tilde{\tau}'_{bipk} - g_{jcpa}\,\tilde{\tau}'_{pibk}\}$ $+ P_{bj,ck}\{g_{kpib}\tilde{\tau}'_{ajcp} - g_{pcib}\,\tilde{\tau}'_{ajpk} + g_{ipkb}\,\tilde{\tau}'_{apcj}\}$
$[[[\hat{H},T_{ai}],E_{bj}],T_{ck}]$	=	$+ P_{ck,ai}\{g_{icjq}\,e_{akbq} - g_{icpb}\,e_{akpj}\}$ $+ P_{bj,ck}\{g_{iqkb}\,\tau_{aqcj} - g_{pajc}\,\tau_{pibk}\}$ $+ P_{ai,bj}\{g_{kqja}\,\tau_{cqbi} - g_{pcja}\,\tau_{pkbi}\}$
$[\hat{V}^z_{SOC}, E_{ai}]$	=	$\hat{V}^z_{pa}\,T_{pi} - \hat{V}^z_{ip}\,T_{ap}$
$[\hat{V}^z_{SOC}, T_{ai}]$	=	$\hat{V}^z_{pa}\,E_{pi} - \hat{V}^z_{ip}\,E_{ap}$
$[[\hat{V}^z_{SOC}, E_{ai}], E_{bj}]$	=	$[[\hat{V}^z_{SOC}, T_{ai}], T_{bj}] = -\hat{V}^z_{ja}\,T_{bi} - \hat{V}^z_{ib}\,T_{aj}$
$[[\hat{V}^z_{SOC}, T_{ai}], E_{bj}]$	=	$[[\hat{V}^z_{SOC}, E_{ai}], T_{bj}] = -\hat{V}^z_{ja}\,E_{bi} - \hat{V}^z_{ib}\,E_{aj}$

perturbation operators $\tilde{X} = \sum_{pq} \tilde{V}^X_{pq}\,E_{pq}$ correspond to the commutator of the Hamiltonian where only the one-electron part $\tilde{h}_{pq}\,E_{pq}$ is considered. Commutators for the triplet one-electron perturbation operators $\tilde{V}^z_{SOC} = \sum_{pq} \tilde{V}^z_{pq}\,T_{pq}$ are listed in Table 6. For a more compact notation, we introduced singlet and triplet two-electron excitation operators to the commutators of the Hamiltonian

$$e_{pqrs} = E_{pq}E_{rs} - \delta_{qr}E_{ps} \tag{A2}$$

$$\tilde{\tau}_{pqrs} = E_{pq}T_{rs} - \delta_{qr}T_{ps} \tag{A3}$$

$$\tilde{\tau}'_{pqrs} = T_{pq}E_{rs} - \delta_{qr}T_{ps} = \tilde{\tau}_{rspq} \tag{A4}$$

DOI: 10.1021/acs.jctc.5b01197
J. Chem. Theory Comput. 2016, 12, 1892−1904

Table 7. Commutators of the Operators $\hat{H}$ and $\hat{V}^z_{SOC}$ with One-Electron Singlet and Triplet Excitation Operators Acting on the Hartree−Fock State

$[\hat{H},T_{ai}]\|HF\rangle$	=	$(F_{ba}\ T_{bi} - F_{ij}\ T_{aj} - g_{baij}\ T_{bj})\ \|HF\rangle$
		$+(g_{cabj}\ E_{bj}\ T_{ci} - g_{ikbj}\ E_{bj}\ T_{ak})\ \|HF\rangle$
$[[\hat{H},E_{ai}],T_{bj}]\|HF\rangle$	=	$-P_{ai,bj}\ \{F_{ja}\ T_{bi} + g_{ckja}\ T_{bi}\ E_{ck}\}\|HF\rangle$
		$+\ (-L_{jkia}\ T_{bk} + g_{jkib}\ T_{ak} + L_{iacb}\ T_{cj} - g_{jacb}\ T_{ci})\ \|HF\rangle$
		$-(g_{jkca}\ E_{ci}\ T_{bk} + g_{ikcb}\ E_{ak}\ T_{cj})\ \|HF\rangle$
		$+\ (g_{jkil}\ T_{bk}\ E_{al} + g_{cbda}\ T_{cj}\ E_{di})\ \|HF\rangle$
$[[\hat{H},T_{ai}],T_{bj}]\|HF\rangle$	=	$-2\ g_{ibja}\ \|HF\rangle - P_{ai,bj}\ \{F_{ja}\ E_{bi} - g_{ikja}\ E_{bk} + g_{ibca}\ E_{cj}\ \}\|HF\rangle$
		$-P_{ai,bj}\ \{g_{ckja}\ E_{bi}\ E_{ck} + g_{jkca}\ T_{bk}\ T_{ci}\}\|HF\rangle$
		$+\ (g_{jkil}\ T_{bk}\ T_{al} + g_{cbda}\ T_{cj}\ T_{di})\ \|HF\rangle$
$[[[\hat{H},T_{ai}],E_{bj}],E_{ck}]\|HF\rangle$	=	$-P_{bj,ck}\ \{L_{kcja}\ T_{bi} + L_{kcib}\ T_{aj} - g_{kaib}\ T_{cj}\ \}\|HF\rangle$
		$+P_{bj,ck}\ \{P_{ai,bj}\ \{g_{klib}\ E_{cl}\ T_{aj}\ \} + g_{iljc}\ E_{bk}\ T_{al}\ \}\|HF\rangle$
		$-P_{bj,ck}\ \{P_{ai,bj}\ \{g_{dcib}\ E_{dk}\ T_{aj}\ \} + g_{dajc}\ E_{bk}\ T_{di}\ \}\|HF\rangle$
$[[[\hat{H},T_{ai}],E_{bj}],T_{ck}]\|HF\rangle$	=	$-P_{ck,ai}\ \{L_{icjb}\ E_{ak}\ \}\|HF\rangle$
		$-P_{bj,ck}\ \{-g_{kaib}\ E_{cj}\ \}\|HF\rangle$
		$-P_{ai,bj}\ \{-g_{ickb}\ E_{aj}\ \}\|HF\rangle$
		$+P_{ck,ai}\ \{g_{icjl}\ E_{ak}\ E_{bl} - g_{icdb}\ E_{ak}\ E_{dj}\ \}\|HF\rangle$
		$+P_{bj,ck}\ \{g_{ilkb}\ T_{cj}\ T_{al} - g_{dajc}\ T_{bk}\ T_{dj}\ \}\|HF\rangle$
		$+P_{ai,bj}\ \{g_{klja}\ T_{bi}\ T_{cl} - g_{dcja}\ T_{bi}\ T_{dk}\ \}\|HF\rangle$
$[\hat{V}^z_{SOC}, E_{ai}]\|HF\rangle$	=	$(\hat{V}^z_{ba}\ T_{bi} - \hat{V}^z_{ij}\ T_{aj})\ \|HF\rangle$
$[\hat{V}^z_{SOC}, T_{ai}]\|HF\rangle$	=	$(2\ \hat{V}^z_{ia} + \hat{V}^z_{ba}\ E_{bi} - \hat{V}^z_{ij}\ E_{aj})\ \|HF\rangle$
$[[\hat{V}^z_{SOC}, E_{ai}], E_{bj}]\|HF\rangle$	=	$[[\hat{V}^z_{SOC}, T_{ai}], T_{bj}]\|HF\rangle = (-\hat{V}^z_{ja}\ T_{bi} - \hat{V}^z_{ib}\ T_{aj})\ \|HF\rangle$
$[[\hat{V}^z_{SOC}, T_{ai}], E_{bj}]\|HF\rangle$	=	$[[\hat{V}^z_{SOC}, E_{ai}], T_{bj}]\|HF\rangle = (-\hat{V}^z_{ja}\ E_{bi} - \hat{V}^z_{ib}\ E_{aj})\ \|HF\rangle$

$$\tau_{pqrs} = T_{pq}T_{rs} - \delta_{qr}E_{ps} \tag{A5}$$

The derivation of nested commutators is much more simplified when the two-electron excitation operators above are employed in combination with the following relations:

$$[E_{pq}, E_{ai}] = [T_{pq}, T_{ai}] = -\delta_{pi}E_{aq} + \delta_{qa}E_{pi} \tag{A6}$$

$$[T_{pq}, E_{ai}] = [E_{pq}, T_{ai}] = -\delta_{pi}T_{aq} + \delta_{qa}T_{pi} \tag{A7}$$

$$[e_{pqrs}, T_{ai}] = -\delta_{pi}\tilde{\tau}'_{aqrs} + \delta_{qa}\tilde{\tau}'_{pirs} - \delta_{ri}\tilde{\tau}_{pqas} + \delta_{sa}\tilde{\tau}_{pqri} \tag{A8}$$

$$[\tilde{\tau}_{pqrs}, E_{ai}] = -\delta_{pi}\tilde{\tau}_{aqrs} + \delta_{qa}\tilde{\tau}_{pirs} - \delta_{ri}\tilde{\tau}_{pqas} + \delta_{sa}\tilde{\tau}_{pqri} \tag{A9}$$

$$[\tilde{\tau}'_{pqrs}, E_{ai}] = -\delta_{pi}\tilde{\tau}'_{aqrs} + \delta_{qa}\tilde{\tau}'_{pirs} - \delta_{ri}\tilde{\tau}'_{pqas} + \delta_{sa}\tilde{\tau}'_{pqri} \tag{A10}$$

$$[\tilde{\tau}_{pqrs}, T_{ai}] = -\delta_{pi}\tau_{aqrs} + \delta_{qa}\tau_{pirs} - \delta_{ri}e_{pqas} + \delta_{sa}e_{pqri} \tag{A11}$$

$$[\tilde{\tau}'_{pqrs}, T_{ai}] = -\delta_{pi}e_{aqrs} + \delta_{qa}e_{pirs} - \delta_{ri}\tau_{pqas} + \delta_{sa}\tau_{pqri} \tag{A12}$$

Next, the commutator of the Hamiltonian or perturbation operators of Table 6 must be applied on the HF-SCF reference state, which is compiled in Table 7. Some of the commutators in Table 6 and 7 have already been published in ref 64.

2. Projection onto the (Bi)Orthonormal Basis. The singlet-adapted configuration state functions are given by

$$|(1)^a_i\rangle = {}^1\tau_{ai}|HF\rangle \tag{A13}$$

$$|(1)^{ab}_{ij}\rangle = {}^1\tau_{aibj}|HF\rangle \tag{A14}$$

and form together with the projection manifold

$$\langle(1)^a_i| = \frac{1}{2}\langle HF|{}^1\tau^\dagger_{ai} \tag{A15}$$

$$\langle(1)^{ab}_{ij}| = \frac{1}{3}\langle HF|{}^1\tau^\dagger_{aibj} + \frac{1}{6}\langle HF|{}^1\tau^\dagger_{ajbi} \tag{A16}$$

a biorthonormal basis. For the triplet case, the configuration state functions are

$$|(3)^a_i\rangle = {}^3\tau_{ai}|HF\rangle \tag{A17}$$

$$|(+)^{ab}_{ij}\rangle = {}^{(+)}\tau_{aibj}|HF\rangle \tag{A18}$$

$$|(-)^{ab}_{ij}\rangle = {}^{(-)}\tau_{aibj}|HF\rangle \tag{A19}$$

and form together with projection manifold

$$\langle(3)^a_i| = \frac{1}{2}\langle HF|{}^3\tau^\dagger_{ai} \tag{A20}$$

$$\langle(+)^{ab}_{ij}| = \frac{1}{8}\langle HF|{}^{(+)}\tau^\dagger_{aibj} \tag{A21}$$

$$\langle(-)^{ab}_{ij}| = \frac{1}{8}\langle HF|{}^{(-)}\tau^\dagger_{aibj} \tag{A22}$$

an orthonormal basis.[31] For the derivation of RHS vectors with triplet symmetry the two relations from ref 31 are helpful:

$$\langle^{ab}_{ij}(+)|E_{kl}T_{dl}|HF\rangle = \frac{1}{2}P_{ai,bj}\tilde{P}_{ij}\delta_{aibj,ckdl} \tag{A23}$$

$$\langle^{ab}_{ij}(-)|E_{kl}T_{dl}|HF\rangle = \frac{1}{2}\tilde{P}_{ai,bj}\delta_{aibj,ckdl} \tag{A24}$$

with the permutation operators

$$P_{ai,bj}f_{aibj} = f_{aibj} + f_{bjai} \tag{A25}$$

$$\tilde{P}_{ij}f_{aibj} = f_{aibj} - f_{ajbi} \tag{A26}$$

$$\tilde{P}_{ai,bj}f_{aibj} = f_{aibj} - f_{bjai} \tag{A27}$$

Some of the RHS vectors have terms with nonzero contributions from two triplet one-electron excitation operators projected onto the singlet doubles manifold

DOI: 10.1021/acs.jctc.5b01197
J. Chem. Theory Comput. 2016, 12, 1892−1904

$$\langle {}^{ab}_{ij}(1)|T_{ck}T_{dl}|\mathrm{HF}\rangle = -\frac{1}{3}P_{ai,bj}(2\delta_{aibj,cldk} + \delta_{aibj,dlck}) \quad \text{(A28)}$$

■ ASSOCIATED CONTENT

Supporting Information

The Supporting Information is available free of charge on the ACS Publications website at DOI: 10.1021/acs.jctc.5b01197.

Derivation of the spin−orbit two-electron integrals and explicit expressions for the first-order RHS vectors that involve triplet excitation operators, i. e. ξ^z, $\overline{\xi}^z$, $\xi^{f,X}$, $\xi^{f,z}$, and $\overline{\xi}^{f,z}$, are presented as supporting material; additionally, we provide a saddle-point and minimum structure of the dithiosuccineimide T_1 state as well as the S_0 and T_1 equilibrium structures of the *all-cis* and *all-trans* conformer of the phosphorescent emitter **1** (PDF)

■ AUTHOR INFORMATION

Corresponding Authors

*E-mail: b.helmichparis@vu.nl.
*E-mail: christof.haettig@rub.de.
*E-mail: vanWullen@Chemie.Uni-KL.De.

Notes

The authors declare no competing financial interest.

■ ACKNOWLEDGMENTS

The authors gratefully acknowledged financial support by the Deutsche Forschungsgemeinschaft (DFG) through grant no. HA 2588/5 and HE 7427/1-1. C. v. W. acknowledges financial support by DFG through the collaborative research center Sfb/TRR 88 "3MET". B. H. P. thanks Hans Jørgen Aa. Jensen for stimulating discussions and Katharina Krause for technical assistance and discussions on the X2C-CC2 implementation of ref 15.

■ REFERENCES

(1) Kelley, T. W.; Baude, P. F.; Gerlach, C.; Ender, D. E.; Muyres, D.; Haase, M. A.; Vogel, D. E.; Theiss, S. D. *Chem. Mater.* **2004**, *16*, 4413−4422.
(2) Kutzelnigg, W.; Liu, W. *J. Chem. Phys.* **2005**, *123*, 241102. Iliaš, M.; Jensen, H. J. A.; Kellö, V.; Roos, B. O.; Urban, M. *Chem. Phys. Lett.* **2005**, *408*, 210−215. Liu, W.; Peng, D. *J. Chem. Phys.* **2006**, *125*, 044102. Iliaš, M.; Saue, T. *J. Chem. Phys.* **2007**, *126*, 064102.
(3) Dyall, K. G.; Fægri, K. *Introduction to Relativistic Quantum Chemistry*; Oxford University Press, 2007. Saue, T. *ChemPhysChem* **2011**, *12*, 3077−3094. Fleig, T. *Chem. Phys.* **2012**, *395*, 2−15.
(4) Heß, B. A.; Marian, C. M.; Peyerimhoff, S. D. In *Modern Electronic Structure Theory, Part 1*; Yarkony, D., Ed.; World Scientific, 1995; Chapter 4, pp 152−278.
(5) Kleinschmidt, M.; Tatchen, J.; Marian, C. M. *J. Comput. Chem.* **2002**, *23*, 824−833.
(6) Grimme, S.; Waletzke, M. *J. Chem. Phys.* **1999**, *111*, 5645−5655.
(7) Ågren, H.; Vahtras, O.; Minaev, B. *Advances in Quantum Chemistry*; Academic Press, Inc., 1996; Vol. *27*; pp 71−162.
(8) Langhoff, S. R.; Davidson, E. R. *J. Chem. Phys.* **1976**, *64*, 4699−4710.
(9) Vahtras, O.; Ågren, H.; Jørgensen, P.; Jensen, H. J. A.; Helgaker, T.; Olsen, J. *J. Chem. Phys.* **1992**, *96*, 2118−2126.
(10) Christiansen, O.; Gauss, J.; Schimmelpfennig, B. *Phys. Chem. Chem. Phys.* **2000**, *2*, 965−971.
(11) Vahtras, O.; Ågren, H.; Jørgensen, P.; Jensen, H. J. A.; Helgaker, T.; Olsen, J. *J. Chem. Phys.* **1992**, *97*, 9178−9187.
(12) Christiansen, O.; Gauss, J. *J. Chem. Phys.* **2002**, *116*, 6674−6686.
(13) Tunell, I.; Rinkevicius, Z.; Vahtras, O.; Sałek, P.; Helgaker, T.; Ågren, H. *J. Chem. Phys.* **2003**, *119*, 11024−11034.
(14) Saue, T.; Jensen, H. J. A. *J. Chem. Phys.* **2003**, *118*, 522−536.
(15) Krause, K.; Klopper, W. *J. Chem. Phys.* **2015**, *142*, 104109.
(16) Hess, B. A.; Marian, C. M.; Wahlgren, U.; Gropen, O. *Chem. Phys. Lett.* **1996**, *251*, 365−371.
(17) Marian, C. M.; Wahlgren, U. *Chem. Phys. Lett.* **1996**, *251*, 357−364.
(18) Neese, F. *J. Chem. Phys.* **2005**, *122*, 034107.
(19) Schimmelpfennig, B. *AMFI - An atomic mean field integral program*; University of Stockholm: Stockholm, Sweden, 1996.
(20) Schimmelpfennig, B.; Maron, L.; Wahlgren, U.; Teichteil, C.; Fagerli, H.; Gropen, O. *Chem. Phys. Lett.* **1998**, *286*, 261−266.
(21) Runge, E.; Gross, E. K. U. *Phys. Rev. Lett.* **1984**, *52*, 997−1000. Gross, E. K. U.; Kohn, W. *Phys. Rev. Lett.* **1985**, *55*, 2850−2852. Gross, E.; Kohn, W. In *Density functional theory of many-fermion systems*; Löwdin, P.-O., Ed.; Adv. Quant. Chem.; Academic Press, 1990; Vol. *21*; pp 255−291.
(22) Sałek, P.; Høst, S.; Thøgersen, L.; Jørgensen, P.; Manninen, P.; Olsen, J.; Jansík, B.; Reine, S.; Pawłowski, F.; Tellgren, E.; Helgaker, T.; Coriani, S. *J. Chem. Phys.* **2007**, *126*, 114110. Coriani, S.; Høst, S.; Jansík, B.; Thøgersen, L.; Olsen, J.; Jørgensen, P.; Reine, S.; Pawłowski, F.; Helgaker, T.; Sałek, P. *J. Chem. Phys.* **2007**, *126*, 154108.
(23) Iikura, H.; Tsuneda, T.; Yanai, T.; Hirao, K. *J. Chem. Phys.* **2001**, *115*, 3540−3544. Yanai, T.; Tew, D. P.; Handy, N. C. *Chem. Phys. Lett.* **2004**, *393*, 51−57.
(24) Christiansen, O.; Koch, H.; Jørgensen, P. *Chem. Phys. Lett.* **1995**, *243*, 409−418.
(25) Schreiber, M.; Silva-Junior, M. R.; Sauer, S. P. A.; Thiel, W. *J. Chem. Phys.* **2008**, *128*, 134110.
(26) Winter, N. O. C.; Graf, N. K.; Leutwyler, S.; Hättig, C. *Phys. Chem. Chem. Phys.* **2013**, *15*, 6623−6630.
(27) Hättig, C.; Weigend, F. *J. Chem. Phys.* **2000**, *113*, 5154−5161.
(28) Herzberg, G. *Molecular Spectra and Molecular Structure: Electronic Spectra and Electronic Structure of Polyatomic Molecules*; Van Nostrand, Princeton, NJ, 1966; pp 417−419.
(29) Hättig, C.; Christiansen, O.; Jørgensen, P. *J. Chem. Phys.* **1998**, *108*, 8331−8354.
(30) Christiansen, O.; Jørgensen, P.; Hättig, C. *Int. J. Quantum Chem.* **1998**, *68*, 1−52.
(31) Hald, K.; Hättig, C.; Yeager, D. L.; Jørgensen, P. *Chem. Phys. Lett.* **2000**, *328*, 291−301.
(32) Helgaker, T.; Jørgensen, P.; Olsen, J. *Molecular Electronic-Structure Theory*; Wiley: New York, 2000; Chapter 2, pp 44−45.
(33) Marian, C. M. *Reviews in Computational Chemistry*; John Wiley & Sons, Inc., 2001; Vol. *17*; pp 99−204.
(34) TURBOMOLE, development version. 2015; For further information, see http://www.turbomole.com (accessed January 25, 2016).
(35) Friese, D. H.; Hättig, C.; Ruud, K. *Phys. Chem. Chem. Phys.* **2012**, *14*, 1175−1184.
(36) Koch, H.; de Merás, A. S.; Helgaker, T.; Christiansen, O. *J. Chem. Phys.* **1996**, *104*, 4157−4165.
(37) Hättig, C.; Köhn, A.; Hald, K. *J. Chem. Phys.* **2002**, *116*, 5401−5410.
(38) Hättig, C.; Köhn, A. *J. Chem. Phys.* **2002**, *117*, 6939−6951.
(39) Neese, F. *Wiley Interdisciplinary Reviews: Computational Molecular Science* **2012**, *2*, 73−78.
(40) Friese, D. H.; Winter, N. O. C.; Balzerowski, P.; Schwan, R.; Hättig, C. *J. Chem. Phys.* **2012**, *136*, 174106.
(41) Almlöf, J. *Chem. Phys. Lett.* **1991**, *181*, 319−320.
(42) Ruud, K.; Schimmelpfennig, B.; Ågren, H. *Chem. Phys. Lett.* **1999**, *310*, 215−221.
(43) Jansson, E.; Norman, P.; Minaev, B.; Ågren, H. *J. Chem. Phys.* **2006**, *124*, 114106−1.
(44) Häser, M.; Ahlrichs, R. *J. Comput. Chem.* **1989**, *10*, 104−111.
(45) Peng, D.; Middendorf, N.; Weigend, F.; Reiher, M. *J. Chem. Phys.* **2013**, *138*, 184105.
(46) See manual of ORCA version 3.0.1 for further technical details
(47) Eichkorn, K.; Treutler, O.; Öhm, H.; Häser, M.; Ahlrichs, R. *Chem. Phys. Lett.* **1995**, *240*, 283−290. Eichkorn, K.; Treutler, O.;

DOI: 10.1021/acs.jctc.5b01197
J. Chem. Theory Comput. 2016, 12, 1892−1904

Öhm, H.; Häser, M.; Ahlrichs, R. *Chem. Phys. Lett.* **1995**, *242*, 652−660.
(48) TURBOMOLE V7.0 2015, a development of University of Karlsruhe and Forschungszentrum Karlsruhe GmbH, 1989−2007, TURBOMOLE GmbH, since 2007; available from http://www.turbomole.com (accessed January 25, 2016).
(49) Dunning, T. H. *J. Chem. Phys.* **1989**, *90*, 1007−1023.
(50) Kendall, R. A.; Dunning, T. H.; Harrison, R. J. *J. Chem. Phys.* **1992**, *96*, 6796−6806.
(51) Weigend, F.; Häser, M.; Patzelt, H.; Ahlrichs, R. *Chem. Phys. Lett.* **1998**, *294*, 143−152. Weigend, F.; Ahlrichs, R. *Phys. Chem. Chem. Phys.* **2005**, *7*, 3297−3305.
(52) Weigend, F.; Köhn, A.; Hättig, C. *J. Chem. Phys.* **2002**, *116*, 3175−3183.
(53) Hellweg, A.; Hättig, C.; Höfener, S.; Klopper, W. *Theor. Chem. Acc.* **2007**, *117*, 587−597.
(54) Weigend, F. *J. Comput. Chem.* **2008**, *29*, 167−175.
(55) Grimme, S. *J. Comput. Chem.* **2006**, *27*, 1787−1799. Grimme, S.; Antony, J.; Ehrlich, S.; Krieg, H. *J. Chem. Phys.* **2010**, *132*, 154104.
(56) Perdew, J. P.; Ernzerhof, M.; Burke, K. *J. Chem. Phys.* **1996**, *105*, 9982−9985. Adamo, C.; Barone, V. *J. Chem. Phys.* **1999**, *110*, 6158−6170.
(57) Häser, M.; Almlöf, J. *J. Chem. Phys.* **1992**, *96*, 489−494.
(58) Huber, K.; Herzberg, G. In *NIST Chemistry WebBook, NIST Standard Reference Database Number 69*; Linstrom, P., Mallard, W., Eds.; National Institute of Standards and Technology: Gaithersburg MD, 2015; data prepared by Gallagher, J. W. and Johnson, R. D., III.
(59) Taherian, M.; Maki, A. *Chem. Phys. Lett.* **1983**, *96*, 541−546. Safarzadeh-Amiri, A.; Verrall, R. E.; Steer, R. P. *Can. J. Chem.* **1983**, *61*, 894−900. Szymanski, M.; Steer, R.; Maciejewski, A. *Chem. Phys. Lett.* **1987**, *135*, 243−248.
(60) Kleinschmidt, M.; Tatchen, J.; Marian, C. M. *J. Chem. Phys.* **2006**, *124*, 124101.
(61) Köhn, A.; Hättig, C. *J. Chem. Phys.* **2003**, *119*, 5021−5036.
(62) Chaudhuri, D.; Sigmund, E.; Meyer, A.; Röck, L.; Klemm, P.; Lautenschlager, S.; Schmid, A.; Yost, S. R.; Van Voorhis, T.; Bange, S.; Höger, S.; Lupton, J. M. *Angew. Chem., Int. Ed.* **2013**, *52*, 13449−13452.
(63) Luzanov, A. V.; Sukhorukov, A. A.; Umanskii, V. É. *Theor. Exp. Chem.* **1976**, *10*, 354−361. Martin, R. L. *J. Chem. Phys.* **2003**, *118*, 4775−4777.
(64) Hald, K. Molecular properties in Coupled-Cluster theory. Ph.D. Thesis, Kemisk Institut, Aarhus Universitet, Arhaus, Denmark, 2002.

DOI: 10.1021/acs.jctc.5b01197
J. Chem. Theory Comput. 2016, 12, 1892−1904